238 (2024) 212851

Contents lists available at ScienceDirect

Geoenergy Science and Engineering

journal homepage: www.sciencedirect.com/journal/geoenergy-science-and-engineering

A novel deep learning method based on 2-D CNNs and GRUs for permeability prediction of tight sandstone

Yinhong Tian [a,b,*], Guiwen Wang [a,b,**], Hongbin Li [a,b], Yuyue Huang [a,b], Fei Zhao [a,b], Yunlong Guo [d], Jie Gao [a,c], Jin Lai [a,b]

[a] National Key Laboratory of Petroleum Resources and Engineering, China University of Petroleum (Beijing), Beijing, 102249, China
[b] College of Geosciences, China University of Petroleum (Beijing), Beijing, 102249, China
[c] College of Geophysics, China University of Petroleum (Beijing), Beijing, 102249, China
[d] China Tarim Oilfield Company, PetroChina, Korla, 841000, China

ARTICLE INFO

Keywords:
Tight sandstone reservoir
Permeability prediction
Deep learning
Two-dimensional convolutional neural network (2-D CNN)
Gated recurrent unit (GRU)
Geological feature map

ABSTRACT

The accurate calculation of tight sandstone reservoir permeability is crucial for optimizing production and maximizing natural gas recovery. Traditional physical model-based permeability calculation methods heavily rely on core experimental parameters. However, petrophysical experiments are costly, prompting the development of fast and reliable reservoir permeability prediction methods. In this paper, a novel deep learning model that combines two-dimensional convolutional neural network (2-D CNN) model and gated recurrent neural network is proposed to predict tight sandstone reservoir permeability. The 1-D conventional well logs data is converted into the 2-D geological feature map to fit the model's input dimension. The TimeDistributed layer wrapping technology is used to couple the 2-D CNN and GRU to extract comprehensive features of geological feature maps. By training the model, a depth nonlinear mapping between the spatial and temporal features in the well logs data and permeability is established. The model is divided into two subnetworks, 2-D CNNs and GRUs, which are used to compare and analyze the functions of different modules in the proposed model. Additionally, two traditional machine learning algorithms, SVM and XGBoost, are also introduced as comparison models. Four regression evaluation metrics are used to quantify the predictive performance of different models. The test results in a blind well demonstrate that the proposed method outperforms the comparison models in predicting permeability, with a coefficient of determination (R^2) of 0.9305, a root mean square error (RMSE) of 0.0895, a mean squared error (MSE) of 0.0080, and a mean absolute error (MAE) of 0.0725. This model can provide insight into the petrophysical characteristics of reaction reservoirs based on conventional well logs data and can accurately estimate reservoir permeability under limited core data, which has great application potential in improving the exploration accuracy of unconventional oil and gas resources.

1. Introduction

Permeability, a crucial parameter in the petroleum industry, plays a pivotal role in reservoir characterization and productivity evaluation (Aïfa et al., 2014a; Zhou et al., 2020a; Seyyedattar et al., 2021). However, accurately calculating permeability in tight sandstone reservoirs faces multiple challenges due to the complexity and heterogeneity resulting from intense diagenetic modifications (Aïfa et al., 2014b; Qin et al., 2020; Kardani et al., 2021; Yang et al., 2021; Liu et al., 2022). Previous permeability prediction methods, such as the Kozeny-Carmen equation and Hydraulic Flow Units, which rely on petrophysical models, have inherent limitations (Carman, 1997; Babak and Resnick, 2016; Zhang et al., 2018; El-Gendy et al., 2022; Gao et al., 2022). Moreover, these empirical relationships heavily depend on costly and time-consuming laboratory core experiments, resulting in scarce core analysis data for any given reservoir (Ahmadi, 2015; Zheng et al., 2021; Huo et al., 2022; Mohammadian et al., 2022).

To address these challenges, there is a need for a faster, accessible, and capable method to predict permeability in tight sandstone reservoirs with high heterogeneity. Machine learning (ML) techniques, as powerful

* Corresponding author. China University of Petroleum-Beijing, 18 Fuxue Road, Changping, Beijing, 102249, China.
** Corresponding author. China University of Petroleum (Beijing), China.
E-mail addresses: cupbtyh@163.com (Y. Tian), wanggw@cup.edu.cn (G. Wang).

https://doi.org/10.1016/j.geoen.2024.212851
Received 28 June 2023; Received in revised form 25 February 2024; Accepted 23 April 2024
Available online 27 April 2024

data mining tools, have shown successful applications in geoscience (Handhal et al., 2020; Ameur-Zaimeche et al., 2022; Chen et al., 2022; Mustafa et al., 2022; Niu et al., 2022; Saporetti et al., 2022). ML models are ideally suited for predicting permeability, as they can explore the complex nonlinear mappings between input variables and permeability (Wu et al., 2018; Otchere et al., 2021). Well logs, which contain extensive information about the petrophysical properties of the reservoir, are commonly available in hydrocarbon fields. Consequently, many studies have utilized different combinations of well logs as input data for permeability prediction models. For instance, Ali Ahmadi et al. (2013) proposed an artificial neural network (ANN) model optimized by hybrid genetic algorithm and particle swarm optimization (HGAPSO) for permeability prediction in shale reservoirs. Rafik and Kamel (2017) demonstrated the feasibility of utilizing logging data, including gamma ray, acoustic transit-time (DT), resistivity (LLD), density (RHOB), neutron (NPHI), and water saturation, to predict permeability in sandstone reservoirs. Gu et al. (2018) employed a continuous restricted Boltzmann machine (CRBM) to extract new data features from logging data and developed a data-driven permeability prediction model based on support vector regression (SVR) optimized by particle swarm optimization (PSO). Sen et al. (2021a) applied the Random Forest (RF) regression method with nine conventional well logs for permeability prediction in the North Razzak Oilfield, Egypt. Zhang et al. (2021a) combined ML algorithms with empirical permeability prediction equations and established a permeability prediction model driven by gamma ray, bulk density (DEN). These studies have shown the potential of ML in permeability prediction. However, most of these studies focused on developing robust models without fully exploiting the information contained in well logs about reservoir characteristics in spatial and temporal scales (Al Khalifah et al., 2020; Osogba et al., 2020; Bai et al., 2022; Kamali et al., 2022). Additionally, traditional ML methods have limitations that cannot be easily addressed by tuning hyperparameters.

Deep learning, an extension of classical ML, overcomes the limitations of traditional ML by incorporating powerful feature extraction and structural modeling techniques, such as convolutional neural networks (CNNs) and recurrent neural networks (RNNs) (Bergen et al., 2019). CNNs are effective in processing 2D data, such as image data (Li et al., 2023b; Nagao et al., 2023), while RNNs are well-suited for analyzing continuous time-series data (Wang et al., 2022; Dong et al., 2023; Shi et al., 2023), like well logs. Researchers have increasingly applied DL models based on CNNs or RNNs to predict reservoir parameters, including permeability. Sudakov et al. (2019) demonstrated the excellent ability of 3-D CNNs in predicting permeability based on X-ray microtomography scans of sandstone subsamples. Yu et al. (2020) addressed the limitations of traditional ML methods in processing image data by employing a 2-D CNN model with scanning electron microscopy images of sandstone to predict permeability in water-bearing sandstone reservoirs. Chen and Zhang (2020) proposed an end-to-end DL model based on LSTM to predict geomechanical parameters, demonstrating the model's ability to incorporate spatial dependence in conventional well logs. Zhang et al. (2022) utilized an autoencoder-based CNN trained on synthetic high-resolution porous media images to achieve fast permeability prediction. Their study successfully captured the implicit connection between permeability and 2-D porous media image data. Despite these advancements, the aforementioned studies focused on the application of a single DL module (CNNs or RNNs), without fully exploiting the high expansibility and flexibility of DL. Combining CNNs and RNNs algorithmically allows for the extraction of high-dimensional features from input data at multiple scales simultaneously. Wang and Cao (2021) developed an integrated DL model that extracted local correlations from conventional well logs using 1-D CNNs and inputted the features directly into GRU for learning trend and context features with respect to depth. However, the use of 1-D CNNs only mapped different well logs at certain depth points to high-dimensional features, resulting in a loss of temporal information compared to the original logging curves. Moreover, the utilization of interpretation porosity instead of core porosity as label data for model regression is not convincing. Similarly, Yang et al. (2022) proposed a hybrid model combining 1-D CNNs and LSTMs to explore the nonlinear relationship between permeability and various logging data, achieving good prediction performance in blind well testing. Nevertheless, the drawbacks associated with 1-D CNNs in processing well logs remain unresolved.

In the realm of permeability prediction for tight sandstone reservoirs, existing research has predominantly focused on the integration of well logs with machine learning techniques. However, a critical gap in the literature remains: the comprehensive capture of both the spatial and temporal intricacies inherent in well logs. This study is motivated by the imperative to bridge this gap, endeavoring to cultivate a deeper comprehension of the intricate interplay between well logs and deep learning models. The overarching goal is to present an innovative and efficient approach for permeability prediction tailored to the unique challenges of tight sandstone reservoirs. In pursuit of this objective, we introduce a novel DL model, denoted as TimeDistributed-convolutional neural networks-gated recurrent units (TDCNNs-GRUs), specially engineered to harness the wealth of information contained within well logs. Our model architecture is twofold, comprising two principal modules: 2-D Convolutional Neural Networks (2D-CNNs) and Gated Recurrent Units (GRUs). The 2-D CNNs component excels in the extraction of high-dimensional spatial features from geological feature images meticulously derived from well logs, as demonstrated in prior work (Zhong et al., 2019). These geologic feature images serve as tailored representations of well logs at discrete depths, capturing the nuanced reservoir characteristics that align seamlessly with the innate capabilities of 2-D CNNs. In concert with 2-D CNNs, the GRUs are meticulously designed to model the temporal aspects inherent to the extracted spatial features. To ensure the faithful preservation of temporal dynamics while simultaneously capturing the rich high-dimensional features encapsulated within geological feature maps at each depth, we introduce a TimeDistributed layer wrapping technique within the 2-D CNNs.

As a testament to the robustness and efficacy of our proposed TDCNNs-GRUs model, we conduct an extensive comparative analysis against contemporary state-of-the-art models and classical permeability prediction approaches, including 2-D CNNs, GRUs, Support Vector Machines (SVM), and XGBoost. The performance evaluation is grounded in the empirical analysis of real-world core data obtained from the Ordos Basin.

This study not only aims to advance the domain of permeability prediction but also seeks to elevate the broader understanding of the intricate interactions between machine learning models and geological data, thus contributing substantially to the reservoir characterization field and facilitating more accurate predictions in the context of unconventional oil and gas resources.

2. Geological settings

The dataset employed in this study was sourced from the Hangjinqi area (Fig. 1(a)), which is located within the Ordos Basin (Zou et al., 2013; Xu et al., 2018; Tan et al., 2023). The Ordos Basin, positioned on the western margin of the Paleozoic North China Block (NCB) overlying an Archean-Proterozoic basement, is characterized as a multicyclic intraplate cratonic basin (Zhang et al., 2017; Xu et al., 2018) (Fig. 1(a)). The basin is geographically bounded by the Yin Mountain to the north, Lvliang Mountain to the east, Qinling orogenic belt to the south, and Liupan and Helan Mountains to the west (Qiu et al., 2019; Dong et al., 2022; Sun et al., 2023). The Ordos Basin can be categorized into six primary tectonic units: the Yimeng Uplift, Western Thrust Belt, Tianhuan Depression, Yishan Slope, Jinxi Fold Belt, and Weibei Uplift (Yang et al., 2005) (Fig. 1(a)). The prevailing structural configuration of the basin is marked by a significant asymmetric syncline, featuring a broad and gentle eastern flank, in contrast to a steep and narrow western flank, with mountainous terrain flanking both sides (Xiao et al., 2005). The Hangjinqi area, located within the northern part of the Ordos Basin, falls

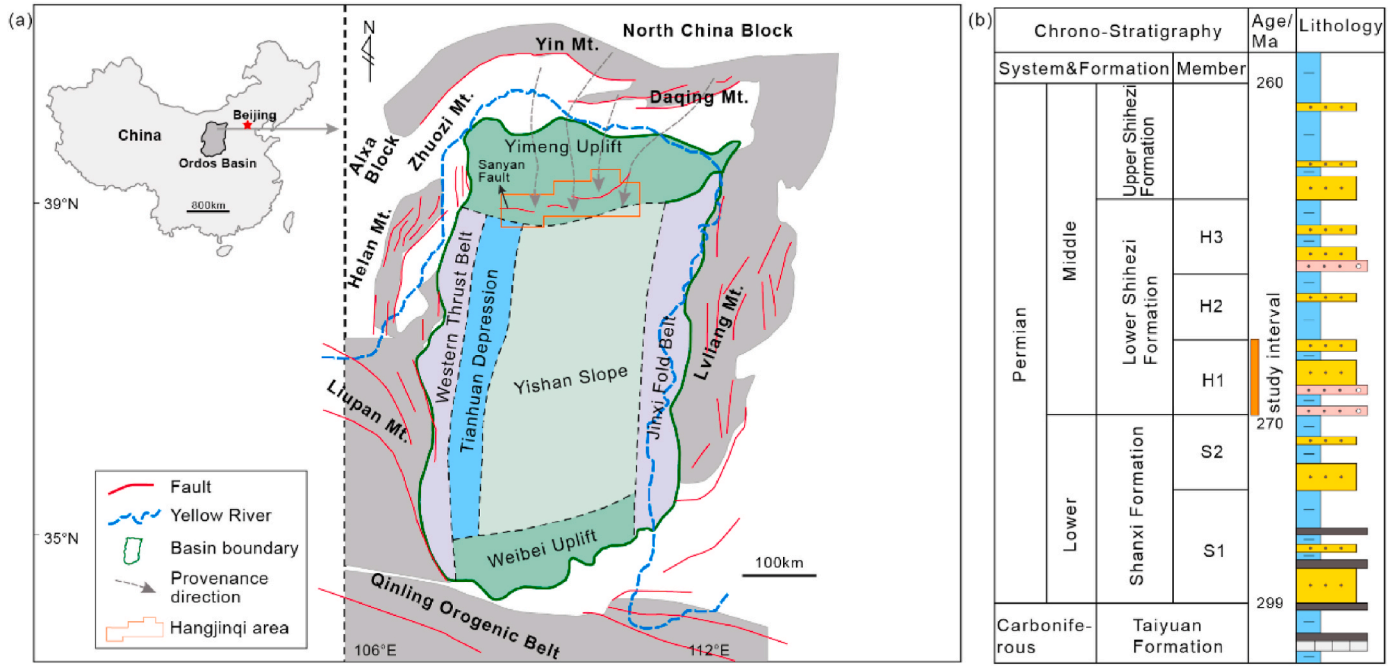

Fig. 1. (a) Location of the Hangjinqi area, and the structural units in the Ordos Basin; (b) stratigraphy of the Shihezi Formation (Modified after Tan et al., 2023).

within the Yimeng Uplift zone. This region is characterized by the presence of three major faults, exhibiting strikes that range from west to east and southwest to northeast (Liu et al., 2020). Among these, the Borjanghazi fault, the largest fault in the area, has undergone several evolutionary stages, including formation during the Caledonian-Early Hercynian period, extrusive-thrusting during the Indosinian-Early Yanshanian period, and strike-slip tearing in the Middle-Late Yanshanian periods (Li et al., 2015) (Fig. 1(a)). Over an extended period, geologists have dedicated their research efforts to studying dense sandstone reservoirs within the Hangjinqi area (Tan et al., 2023). Notably, the focus has been on a tight sandstone gas reservoir located in the Lower Shihezi (Fig. 1(b)) Formation of the Upper Paleozoic Permian, exhibiting significant potential for natural gas production (Wang et al., 2020b).

3. Methodology

3.1. 2-D convolutional neural network

2-D CNNs dominate the field of computer vision, such as image classification (He et al., 2016; Krizhevsky et al., 2017), object detection (Girshick et al., 2014) and semantic segmentation (Ronneberger et al., 2015), due to their unique advantages in image data processing. A convolutional neural network model built for a specific task is typically a recurrent structure, which consisting of a sequence of convolutional and pooling layers (Sakhavi et al., 2018). The core algorithm of the convolution layer, the convolution operation, is able to capture the local features of the input images and map them to high-dimensional features. Fig. 2 illustrates the procedure of 2-D CNN processing the input data with convolutional layers and pooling layer in detail. The convolutional kernel implements the convolution operation, which the corresponding elements in the input and the convolution kernel are multiplied separately and then summed to obtain a new feature element, and a feature map (Fig. 2(b), (c)) is generated when the convolutional kernel traverses the entire input. The kernel size determines the receptive field and further controls the information abundance of the feature map, while the stride is deployed to change the density of convolving. When the convolution kernel size and the stride are setting to k × k and s × s respectively, and the size of the input is n × n, then the generated feature

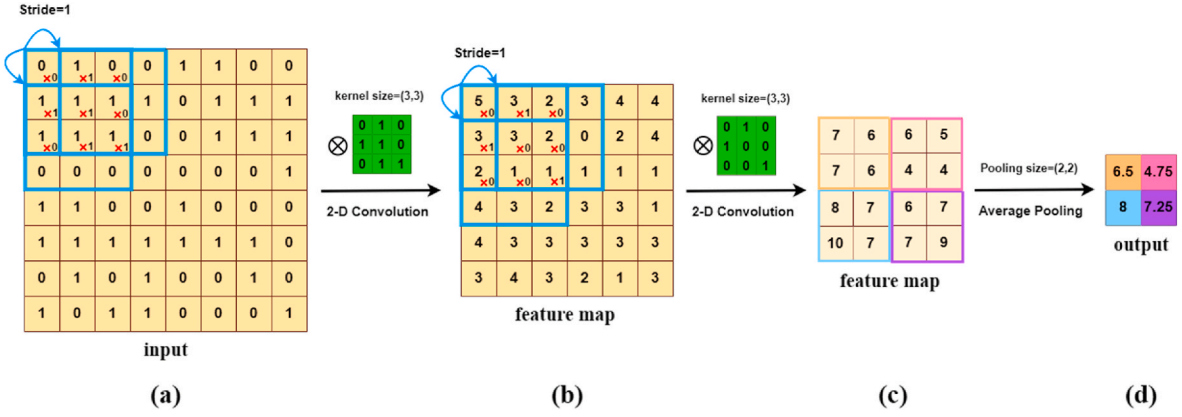

Fig. 2. Example of the computational procedure of a 2-D Convolutional Neural Network (CNN) utilizing two convolutional kernels of size 3 × 3, a stride of 1, and zero padding of 0. (a) The input size is 8 × 8. (b) After the first convolution operation, a feature map of size 6 × 6 is obtained. (c) The second convolution operation produces a feature map of size 4 × 4. (d) The output after a pooling layer of size 2 × 2, ultimately generating a final output of size 2 × 2.

map size is ($\frac{n-k}{s}+1$; $\frac{n-k}{s}+1$). Two convolutional layers with two different 3 × 3 convolutional kernels are shown in Fig. 2. The first layer mainly extracts the low-level features (e.g., edge features), and the high-level features represent certain properties of the inputs are obtained as the convolutional layers expand. Besides, in order to eliminate the overfitting problem which caused by the numerous features in feature maps, the pooling layer is developed to obviate redundancy (Li et al., 2022). On the other hand, the reduction of features in the feature maps does not affect the effectiveness of its overall features, which due to the translation invariance of the pooling. There are two typical pooling methods, average pooling and max pooling. Thus, in view of the excellent performance of 2-D CNNs in feature extraction, we place several 2-D CNNs as the first module of the TDCNNs-GRUs for initial feature extraction of the inputs.

3.2. Gated recurrent unit

The vanilla RNNs have plagued by the vanishing gradient problem with the long sequence inputs (Dong et al., 2021). To address this intractable issue, the sophisticated units with gating mechanism, i.e., Long short-term memory (LSTM) (Hochreiter and Schmidhuber, 1997) and gated recurrent unit (Cho et al., 2014; Ghazi et al., 2022), have been advanced. In addition, as an upgraded version of LSTM, GRUs have been proved in many studies that achieved comparable performance to LSTMs but simpler and more effective which demands fewer computations (Chung et al., 2014; Wang et al., 2020a). The GRU cell introduce two gating mechanism which namely update gate and reset gate. The graphical illustration of the internal structure of the GRU cell is shown in Fig. 3. The reset gate r_t performs filtering operations on the previous hidden state h_{t-1}, which eliminate the irrelevant information by taking into account the current input x_t. Then the filtered output from the reset gate r_t is coupled with the h_{t-1} and x_t to produce a new hidden state $\widetilde{h}_t$. The update gate Z_t determines which information is discarded from the previous hidden state h_{t-1} and what new information is obtained from the new hidden state $\widetilde{h}_t$. The customized ability of the two gates, such as capture short-term dependencies and preserve long-term dependencies, ensured the next hidden state h_t contains the most potent information and transmit to the next GRU cell (Ikuta and Zhang, 2022). Each step of data processing in the GRU cell is expressed as follows:

$$r_t = \sigma(W_r \bullet [h_{t-1}, x_t] + b_r) \tag{1}$$

$$Z_t = \sigma(W_Z \bullet [h_{t-1}, x_t] + b_Z) \tag{2}$$

$$\widetilde{h}_t = tanh(W_h \bullet [r_t \odot h_{t-1}, x_t] + b_{\widetilde{h}_t}) \tag{3}$$

$$h_t = (1 - Z_t) \odot h_{t-1} + \widetilde{h}_t \odot Z_t \tag{4}$$

where σ is the sigmoid activation function and tanh is another type of activation function, $\odot$ is the Hadamard product operator, which represents the element-wise multiplication of vectors, W_r, W_z, and W_h are the weight matrix in the calculation of the reset gate r_t, the update gate Z_t and the new hidden state $\widetilde{h}_t$, respectively, and b_r, b_Z and $b_{\widetilde{h}_t}$ are the bias of the reset gate r_t, the update gate Z_t and the new hidden state $\widetilde{h}_t$, respectively.

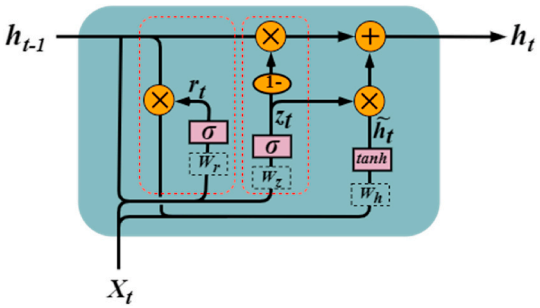

Fig. 3. Structure of the GRU cell.

3.3. Architecture of the TDCNNs-GRUs model

The ability of the constructed DL model to understand the spatio-temporal features in the logging curve is a crucial objective factor for the success of the predictive model (Afrasiabi et al., 2021). We place the 2-D CNNs as a feature extractor by taking account into its extraordinary feature extraction ability. The output of the 2-D CNNs is then taken directly as input to the GRUs to perform the extraction of the temporal features, and eventually the nonlinear mapping relationship between the logging data and the permeability is established during the network training. Although the idea of combining 2-D CNNs and GRUs to build a DL model is logically feasible from the model principle, however, there are two main challenges in its implementation, i.e., the mismatch of data dimension and the incompatibility of different models. The well logs are one-dimensional continuous data, which not fit with the input dimensions of the 2-D CNNs. On the other hand, the GRUs demands input samples with a set timesteps (e.g., well logs at continuous depth points), but the raw data with a fixed timesteps after preprocessing will first pass through the 2-D CNNs, which eliminates the temporal features inherent in the well logs due to the 2-D CNNs process it as a whole rather than separately for each timestep. Therefore, considering the above problem of basic 2-D CNNs, a novel DL model (TDCNNs-GRUs) employs the TimeDistributed function (Qiao et al., 2018; Montaha et al., 2022) to combine 2-D CNNs and GRUs is proposed. The framework of the TDCNNs-GRUs is shown in Fig. 4.

The TDCNNs-GRUs architecture, which we propose in this paper, consists of four concatenated blocks that make up the main structure. The four blocks correspond to four major procedures: geologic feature image conversion, TimeDistributed local spatio-temporal feature extraction, holistic temporal feature extraction and permeability prediction. Firstly, we introduce geologic feature image to deal with the mismatch of data dimensions, and the geological feature image is constructed through a fusion of multiple well logs, specifically including spontaneous potential (SP), gamma ray (GR), shale content (SH), acoustic curve (AC), bulk density (DEN), compensated neutrons (CNL), deep induction resistivity (LLD), and medium induction resistivity (LLS). We segment the normalized well logs and use a sliding window along the depth dimension to convert them into images, which are then combined into a collection of geological feature images. The conversion process is described in detail in the next section. Then, a layer wrapper namely TimeDistributed is used to coordinate the compatibility between two models i.e., 2-D CNNs and GRUs. After data segmentation and conversion and input of samples with a specific timesteps N, the TimeDistributed local spatio-temporal feature extraction layers are used to extract spatio-temporal features of the geological feature image in each timesteps. Utilizing the TimeDistributed wrapper, the local feature extractor is concurrently applied to each geological feature image N_i, as depicted in Fig. 4. The N geological feature images undergo simultaneous and independent local feature extraction processes, which ensures that the processing of each feature is isolated from the others and can be optimized individually. By utilizing 2-D CNNs with a TimeDistributed wrapper, input data containing temporal features can share parameter information of a single convolutional layer. This allows the feature maps of various convolutional layers to share weights, which, in turn, maintains the effective temporal features required for the subsequent GRU model. Consequently, the number of convolutional layer parameters is significantly reduced.

The proposed architecture employs a stack of holistic GRU layers that are built on top of TimeDistributed local spatio-temporal feature extraction layers. This allows the model to effectively capture holistic temporal features between each geological feature image N_i, based on

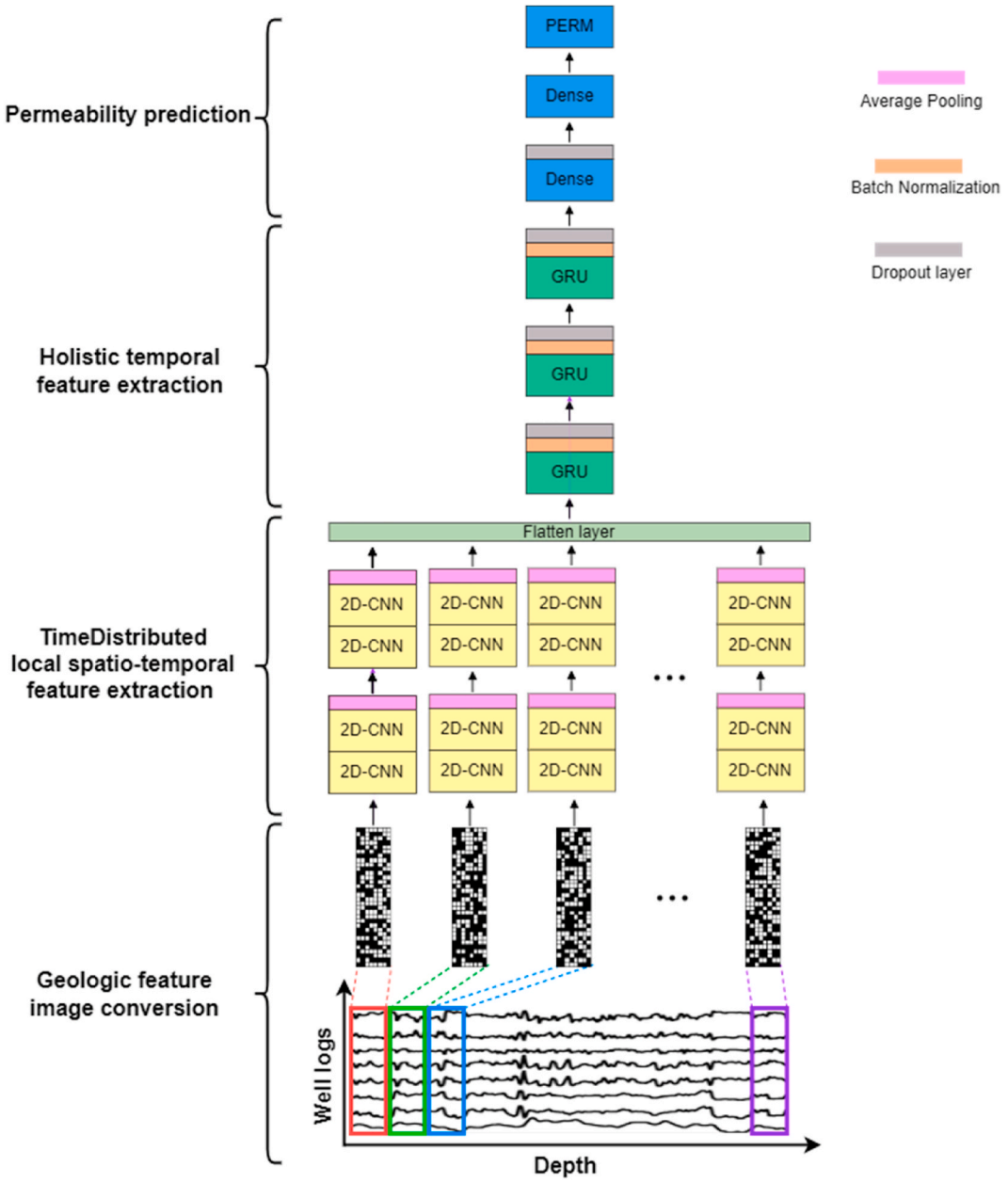

Fig. 4. The framework of the proposed TDCNNs-GRUs model.

the information extracted by the TimeDistributed local spatio-temporal feature extraction layers. The spatio-temporal features processed by GRUs help the model in discerning concealed patterns in challenging frame to-frame sequences. During this process, the extracted features from the 2-D CNNs are fed into the GRUs as a sequence, capturing the long temporal dependencies among the frames of all geological feature images (Arif et al., 2019; Ercolano and Rossi, 2021). To mitigate the issue of internal covariate bias during iterations and improve training efficiency, batch normalization and dropout layers are applied to the output of each GRU layer (Srivastava et al., 2014; Ba et al., 2016). At last, two dense layers are stacked on the top of the TDCNNs-GRUs to obtain the target permeability value. Our objective is to develop a network framework that is both accurate and efficient, while also being capable of generalization across a range of reservoir conditions. To achieve this goal, we employ a combination of several networks for predicting reservoir parameters.

4. Data characterization and analysis

In this section, we provide a comprehensive description of the datasets used in this study, which include conventional logging data and core experimental data utilized for the permeability prediction tasks. Next, we elaborate on the process of generating geological feature maps using logging data. Subsequently, we describe two approaches for evaluating the TDCNN-GRU model's prediction performance: 1) using multiple regression evaluation metrics to analyze the prediction accuracy of the model, and 2) comparing the prediction results with benchmark models that have been proposed and widely used. Additionally, we discuss the network's training, validation, and testing steps, along with detailed information on model parameters and optimization techniques.

4.1. Petrophysical properties data features

The tight sandstone reservoirs of the Lower Permian Lower Shihezi

Formation in Hangjinqi area of Ordos Basin were selected as the experimental site for this study. Measured petrophysical properties data (i.e., label data permeability) of 112 samples were obtained from four wells, with 39 samples of Well J92, 29 samples of Well J95, 21 samples of Well J101, and 23 samples of Well J103, separately. Fig. 5(i) depicts the distribution of permeability values for the entire dataset, presenting the frequency distribution of labeled data in each well. The results indicate that the permeability values range from 0.036 to 1.482 mD, with a mean value of 0.504 mD. It is noteworthy that the majority of the samples (about 45%) exhibit a permeability of less than 0.4 mD, highlighting the intense compaction and diagenesis of the target reservoir in the study area, which poses challenges in accurately predicting permeability. These labeled samples have been utilized as ground truth data for training and testing machine learning models. Furthermore, eight conventional well logs data, namely spontaneous potential (SP), gamma ray, shale content (SH), acoustic curve (AC), bulk density (DEN), compensated neutrons (CNL), deep induction resistivity (LLD), and medium induction resistivity (LLS), have been chosen as input in this study and presented in Fig. 5(a–h). In addition, we chose well J103 as the testing well, while all data from the other three wells were used as training data. Notably, the data from well J103 was not involved in the model training. This operation, rather than randomly splitting the data into a ratio of 0.8:0.2 for training and testing, can truly verify whether the established deep learning model has reliable robustness and generalization in predicting permeability in the study area.

4.2. Generation of geological feature maps

As previously stated, our TDCNNs-GRUs model requires two-dimensional image data as input. However, we currently only have core permeability data and its corresponding eight logging curves data on a specific depth section. To address this issue, we introduce geological images to convert the one-dimensional logging data into two-dimensional picture data. The geological feature images were first defined by Zhong et al. (2019), where they converted five logs corresponding to one depth point into a geological feature map and used it as input data to build a high-precision permeability prediction model based on a two-dimensional convolutional neural network. Although they did not specify the geological significance represented by the geological feature maps, their study demonstrated the rich stratigraphically relevant geological and geophysical information contained in the geological feature maps. Subsequently, Masroor et al. (2022) further demonstrated that the geological feature image contains all the conventional well logs information and their possible interactions, showing that the geological

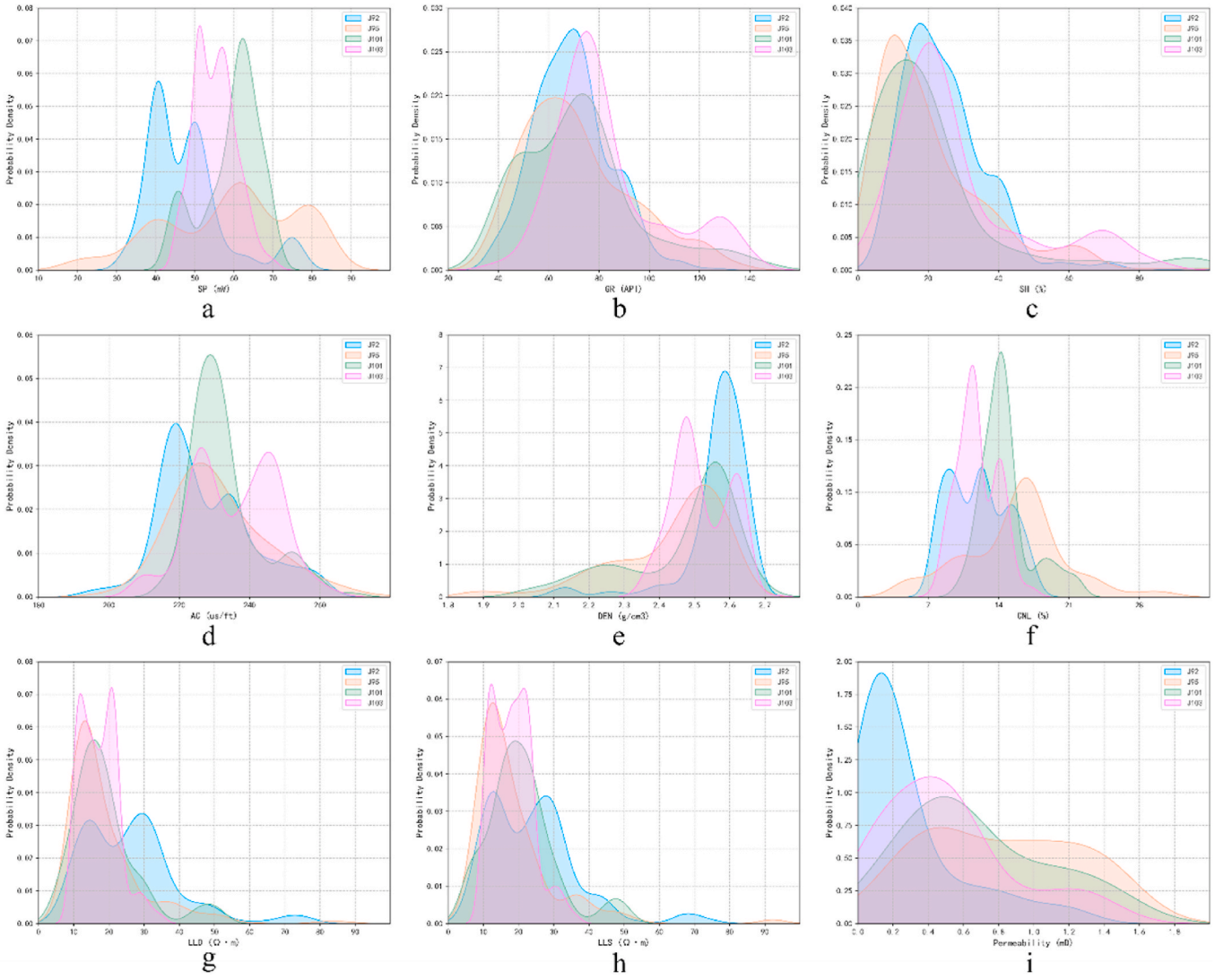

Fig. 5. Probability density of well logs and label data for four wells (J92, J95, J101, and J103) shown in blue, orange, green, and purple colors, respectively. (a)–(h) represent Probability density of eight types of logging data including SP, GR, SH, AC, DEN, CNL, LLD, and LLS. (i) represents Probability density of core data (label data).

feature map contains a wealth of mineable numerical information related to reservoir characteristics.

In order to produce geological feature maps, we convert the decimal values of each feature into binary strings at every depth point. To avoid inconsistencies in the length of the original logging values resulting from their differing magnitudes and value ranges, we first normalize the well logs data and then convert them into 32-bit binary strings. We use Eq. (5) to normalize the well logs. The eight logging curves (Fig. 6(a)), which correspond to the eight petrophysical variables of the formations, are then transformed into eight 32-bit binary strings, which form a geological feature map for each depth point. This generates a matrix of size 8 × 32 consisting of "0″ or "1″ values for each depth point (Fig. 6(b)). Subsequently, we convert the "1″ and "0″ values in the matrix into square binary images with 255 and 0 pixels, respectively. Finally, these images are stacked together to create a geological feature map, a black/white 2-D image (Fig. 6(c)). Each geological feature image is uniquely represented by a black and white image, with each 2-D geological feature map corresponding to the permeability value at a particular depth point (Fig. 6(d)). The conversion process is illustrated in detail in Fig. 6.

$$x' = \frac{(x - x_{min})}{(x_{max} - x_{min})} \tag{5}$$

Recognized as time-series data, the trends exhibited by well logs, coupled with their contextual information, contain invaluable insights into the stratigraphic variations that emerge from intricate depositional and diagenetic processes (Wang et al., 2021; Wu et al., 2021; Yang et al., 2023). Consequently, when extracting features from well log data, it becomes imperative not only to examine the spatial correlations among distinct logging parameters but also to address the depth-dependent variations in these parameters. It should be highlighted that a primary function of our TDCNNs-GRUs model is to extract temporal features from the input data. To achieve this, the input data must consist of a continuous string of 2-D image data. Consequently, during the data pre-processing stage, we establish a timestep of size 13 for the input data, which encompasses 13 sampling points moving upward from the depth that corresponds to the core permeability (the well logs sampling interval in the study area is 0.125m). We collate the images of geological features at 13 successive depth points as one sample data, with the last depth point associated with the core permeability as the label data for that sample. A detailed account of the production of a single sample data is presented in Fig. 7.

4.3. Training process and evaluation metrics

Per the TDCNNs-GRUs model structure diagram in Fig. 4, our constructed model consists of two sets of local feature extraction modules. Each module is composed of two two-dimensional convolutional layers, with rectified linear units (ReLU) as activation functions, and an average pooling layer. Following each local feature extraction module are three Gated Recurrent Unit layers, each of which is followed by a batch normalization layer and one dropout layer. Lastly, the model includes two fully connected layers and one output layer. To attain the optimal hyperparameters for the model, genetic algorithms (Ravandi et al., 2014; Yao et al., 2021; Raji et al., 2022) were employed. Genetic algorithms are a potent tool for optimizing neural network architectures for specific tasks, obviating the need for manual tuning of an abundance of hyperparameters (Aïfa, 2014; Yao et al., 2021; Puentes G et al., 2022; Fu et al., 2023). This approach enhances the efficiency and effectiveness of the optimization process, leading to an improvement in the performance and generalization ability of deep learning models (Deighan et al., 2021). The training process is shown in Fig. 8. During training, we utilized the mean squared error (MSE) loss function to correct prediction errors between the real value and the predicted value. In order to avoid gradient vanishing during network iteration, we implemented early stopping and adaptive learning rate optimization algorithms (Zhu and Iiduka, 2021; Iiduka, 2022). We also used the Adam optimization algorithm, which handles gradient sparsity well (Hassan et al., 2023), to minimize the loss function. We initialized the learning rate for the Adam algorithm to be 0.05. If the prediction error did not decrease for 80 consecutive epochs, the learning rate was reduced by 1% based on the original learning rate. And the training process continued with the new learning rate until the prediction error did not decrease for 100 consecutive epochs, at which point the model was terminated and the best training parameters (i.e., those corresponding to the lowest prediction error) were saved. All experiments were conducted using TensorFlow, with neural network training executed on an Intel(R) Core (TM) i7-8750H CPU. Following the utilization of a genetic algorithm to optimize hyperparameters, the runtime for the training was approximately 12 min. The training was terminated after approximately 640 epochs, as the validation loss exhibited no improvement over the last 100 epochs.

In accordance with Fig. 8, we conducted hyperparameter tuning experiments and ultimately determined the hyperparameters for the TDCNNs-GRUs model, which are listed in Table 1. Notably, the kernel size k_1 for the first two 2-D convolutional layers is (2 × 2), the number of filters f_1 is 16, and the stride s_1 is 1. For the subsequent two 2-D convolutional layers, the kernel size k_2 is (2 × 2), the number of filters f_2 is 64, and the stride s_2 is 1. The sizes of the two average pooling layers are both (2 × 2). Additionally, we set the number of units c in each GRU layer to be uniformly 32, the number of neurons n in the two fully connected layers to be 32 and 8, respectively, and the dropout rate d to be 0.25.

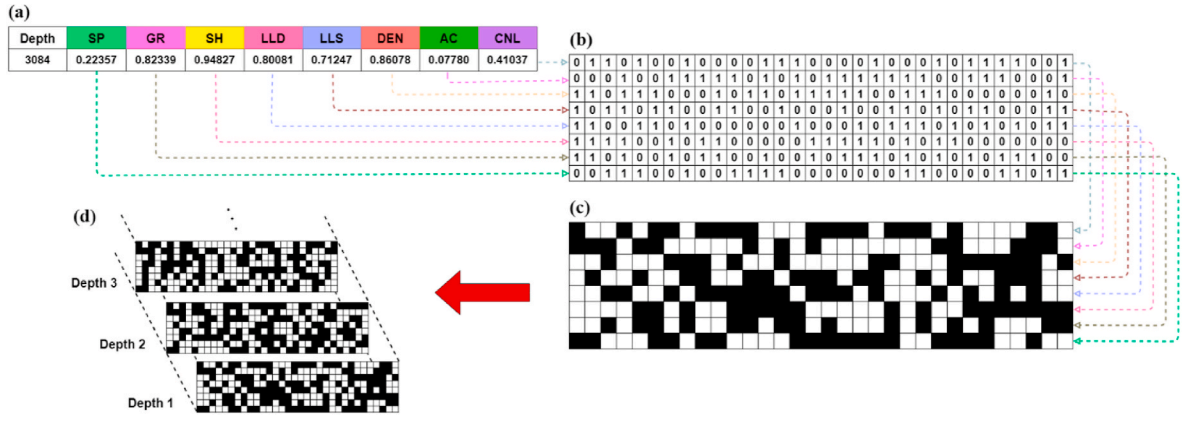

Fig. 6. Schematic representation of the geological feature map conversion process. (a) Values of the eight logging curves at a sampling depth of 3084m. (b) Normalization and conversion of logging data into a 32-bit binary string. (c) Replacement of "1″ values with 255 and "0″ values with 0, followed by conversion to black and white images to generate the corresponding geological feature map for the depth point. (d) Geological feature maps generated for different depths.

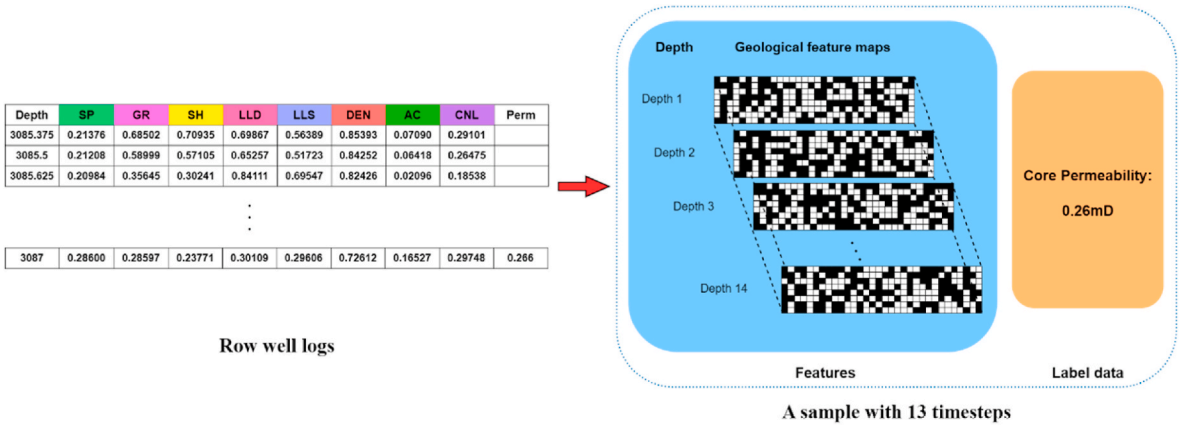

Fig. 7. Schematic diagram of the process of generating a sample dataset consisting of geological feature maps at 13 consecutive depth intervals.

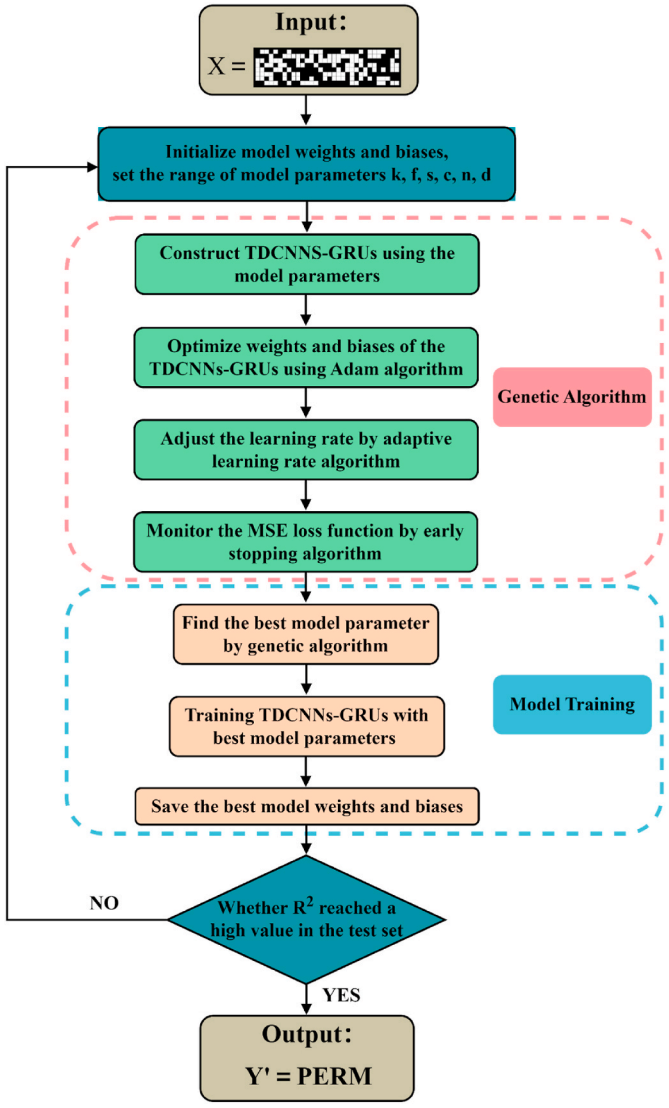

Fig. 8. Flowchart illustrating the training process of the TDCNNs-GRUs model with hyperparameter tuning through the genetic algorithm.

In order to evaluate the performance of our designed network in comparison to baseline and state-of-the-art methods, we have utilized four crucial error-based metrics for quantitative evaluation (Yao et al., 2023). These metrics include Mean Absolute Error (MAE), Mean Squared Error (MSE), Root Mean Squared Error (RMSE) and Coefficient of determination (R^2). The mathematical expressions for these metrics are presented below:

Table 1
Hyperparameters of the TDCNNs-GRUs.

Network hyperparameter	Tuning range	value
Batch size	[8, 128]	16
Initial learning rate	–	0.05
GRU units c	[4, 128]	32
Dropout rate d	[0.1, 0.5]	0.25
Kernel size (first two 2-D convolutional layers) k_1	[2, 4]	2 × 2
Filters (first two 2-D convolutional layers) f_1	[4, 128]	16
Kernel size (last two 2-D convolutional layers) k_2	[2, 4]	2 × 2
Filters (last 2-D convolutional layers) f_1	[4, 128]	64
Stride (four 2-D convolutional layers) s_1, s_2	[1, 3]	1
Neurons (first fully connected layer) n_1	[16, 128]	32
Neurons (last fully connected layer) n_2	[4, 64]	8

$$MAE = \frac{1}{N}\sum_{i=1}^{N}\left|y_i^{'} - y_i\right| \tag{6}$$

$$MSE = \frac{1}{N}\sum_{i=1}^{N}\left(y_i^{'} - y_i\right)^2 \tag{7}$$

$$RMSE = \sqrt{\frac{1}{N}\sum_{i=1}^{N}\left(y_i^{'} - y_i\right)^2} \tag{8}$$

$$R^2 = 1 - \frac{\sum_{i=1}^{N}\left(y_i - y_i^{'}\right)^2}{\sum_{i=1}^{N}\left(y_i - aver(y_i)\right)^2} \tag{9}$$

where $y_i^{'}$ is the true measurement of permeability, $y_i^{'}$ is the predicted value of permeability, aver ($y_i^{'}$) is the average of $y_i^{'}$, i.e., the average of the true measurement of permeability, and N is the number of samples.

The coefficient of determination R^2 is a widely-used statistical tool that gauges the degree to which a model's predictions match the actual observations (Ou et al., 2022). It indicates the fraction of the variance in the dependent variable that can be explained by the independent variable(s) included in the model. Ranging from negative infinity to 1, the R^2 value describes the extent to which the model's predicted values deviate from the observed values. The greater the value of R^2, the more accurately the model represents the data and the more dependable it is deemed to be.

5. Results and discussions

5.1. Assessing model performance: a comparative analysis

In this section, we present the results of permeability prediction using the TDCNNs-GRUs model in the test blind well J103. To provide comparative analysis, we employed two data-driven methods as benchmark models, namely SVM (Baouche et al., 2017; Anifowose et al., 2019) and XGBoost (Zhao et al., 2022), which have been utilized in reservoir permeability prediction tasks. Moreover, to demonstrate the impact of TimeDistributed techniques that can couple CNNs and GRUs on the TDCNNs-GRUs model in terms of permeability prediction performance, we devised the 2-D CNNs (Zhong et al., 2019) (not integrated with GRUs) as a state-of-the-art approach. Additionally, stacked GRUs are also used to evaluate the performance of the developed technique.

The SVM, XGBoost, and GRU models utilize eight well logs (SP, GR, SH, LLD, LLS, AC, DEN, and CNL) as input variables and normalize the input data using Eq. (5). The input data for GRUs and TDCNNs-GRUs are set to have the same time step length to facilitate comparison. The input data for 2-D CNNs is generated from geological feature maps, which are created using the approach explained in Section 3.2. Correlation coefficient matrix analysis between the eight well logging curves and permeability is presented in Fig. 9, which reveals poor correlation between the two. This indicates that it may be challenging to accurately predict permeability based solely on the establishment of a linear or nonlinear mapping relationship between well logging curves and permeability.

Table 2 presents a comparative analysis of the predictive accuracy of the TDCNNs-GRUs method, along with four other techniques, in forecasting permeability in the test well using four performance metrics. The outcomes in the table unequivocally demonstrate that the TDCNNs-GRUs model outperforms the other methods in terms of accuracy, resulting in the most precise permeability predictions in the blind well test. These results collectively highlight the robustness of the proposed approach in accurately forecasting permeability in the study area's tight sandstone reservoirs.

Table 2
Performance evaluation of different models in predicting permeability for test well J102.

Models	MAE (mD)	MSE (mD)	RMSE (mD)	R^2 (−)
Our proposed	0.0725	0.0080	0.0895	0.9305
2-D CNNs (Without GRUs)	0.0711	0.0136	0.1166	0.8695
GRUs (Without 2-D CNNs)	0.1588	0.0466	0.2158	0.7004
SVM	0.1312	0.0272	0.1649	0.6329
XGBoost	0.0973	0.0197	0.1405	0.7924

Fig. 10 presents a comparative analysis of the proposed TDCNNs-GRUs model with other four models. The findings reveal that the proposed model is significantly more accurate in predicting permeability than the state-of-the-art models. The mean square error (MSE) of the proposed method is substantially lower than that of 2-D CNNs, GRUs, SVM, and XGBoost, with values of 0.0136mD, 0.0466mD, 0.0272mD, and 0.0197mD, respectively (Fig. 10(b)). Likewise, the root mean square error (RMSE) of the proposed method is lower than that of the benchmark models, with values of 0.1166mD, 0.2158mD, 0.1649mD, and 0.1405mD, respectively (Fig. 10(c)). The coefficient of determination (R^2) of TDCNNs-GRUs (0.9305) is also higher than that of the benchmark models, which demonstrates the superior performance of the proposed method (Fig. 10(d)). Although 2-D CNNs yield the best prediction results among the benchmark models, TDCNNs-GRUs exhibit improvements of 41.18%, 23.24%, and 7.01% in terms of MSE, RMSE, and R^2, respectively. These results confirm that the temporal features of the logging curves play a critical role in reflecting the geological features and are therefore crucial for accurate permeability prediction.

The permeability of tight sandstone reservoirs is influenced by multiple factors, including rock composition and pore structure (Chen

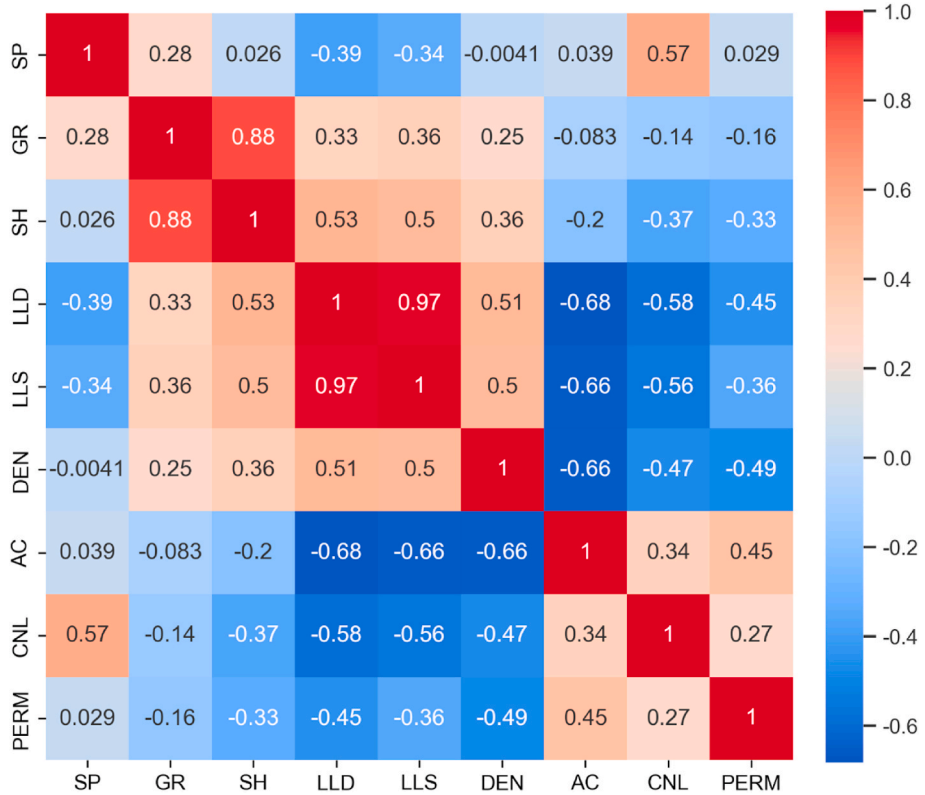

Fig. 9. Correlation coefficient matrix heat map displaying the correlation between eight logging curve data, namely SP, GR, SH, LLD, LLS, DEN, AC, CNL, and core permeability data, PERM.

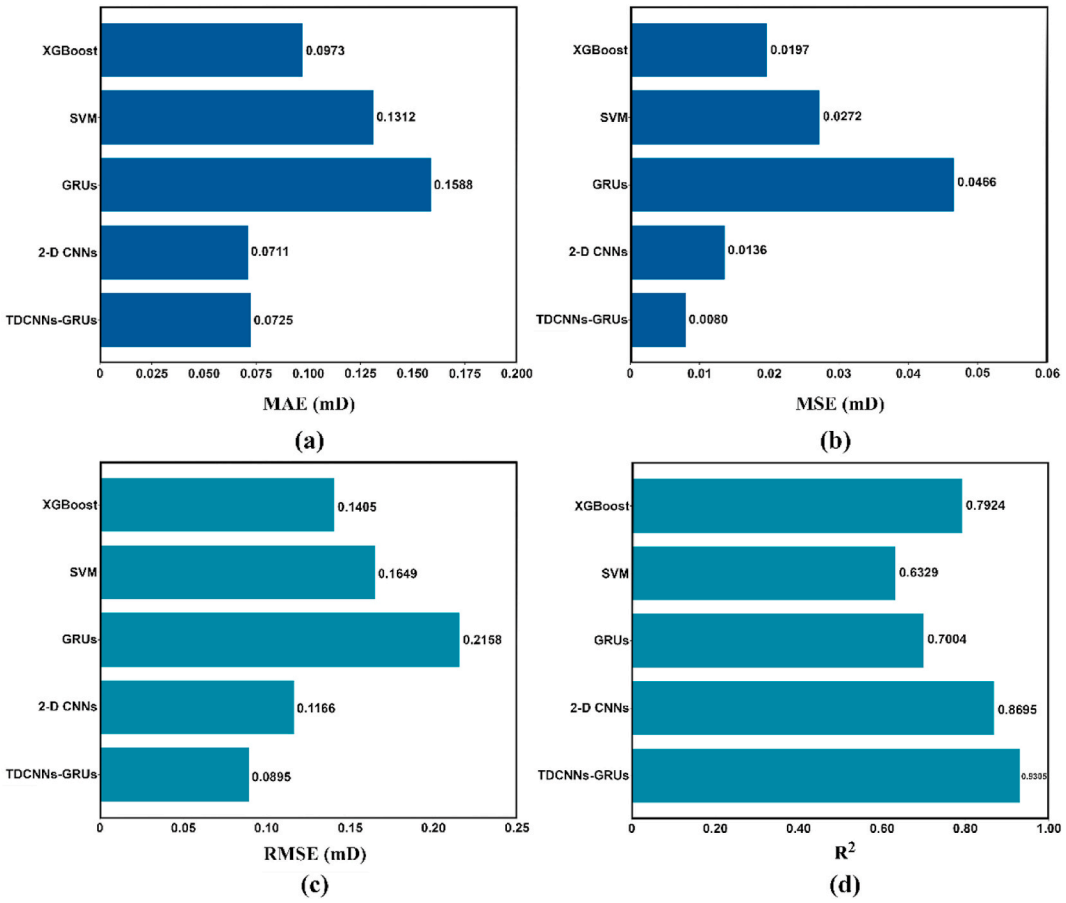

Fig. 10. Comparative analysis of four evaluation metrics for various models in the J102 test well.

et al., 2018), which are indirectly reflected in the logging curve. However, different machine learning methods exhibit varying prediction accuracy despite using the same training and testing data, owing to differences in their model structures. To provide a visual demonstration of the prediction performance of five algorithms in different permeability ranges, Fig. 11 depicts the intersection of the permeability prediction data of different models and the real core permeability data, where the abscissa and ordinate represent the ground truth and prediction results, respectively. A 45° black line along the coordinates indicates that the prediction results are consistent with the ground truth. The results show that the proposed method and 2-D CNNs exhibit good predictions at low permeability, while exhibiting poor predictions at high permeability (as evident from Fig. 11(a) and (b)). Furthermore, a high bias in high permeability predictions is observed since more than 45% of the permeability samples are less than 0.4mD. Interestingly, both models perform relatively well when the permeability is greater than 1mD, which may be due to abnormal high permeability in the local formation that often corresponds to the existence of pore structure mutations or fractures These geological changes cause abnormal logging values, making the statistical sample data more typical, and facilitating the network in learning characteristic information of its samples. Fig. 11 (c) and (d) demonstrate that both GRUs and SVMs exhibit varying degrees of underfitting. Moreover, Fig. 11(e) reveals that the XGBoost algorithm based on the tree model shows an excellent fitting effect in the training dataset, but its results in the test data are not satisfactory, indicating the limitations of traditional machine learning models, which are prone to overfitting.

5.2. *A comparative analysis of permeability prediction models in core well profile: a case study*

Utilizing the five permeability prediction models established earlier, the longitudinal reservoir segments permeability prediction of the JPH381-DY well was performed. The JPH381-DY well is an experimental well located in Hangjinqi area of the Ordos Basin, with the tight sandstone gas reservoir mainly developed in the lower Shihezi Formation. The logging items for JPH381-DY well encompassed eight conventional well logs, including SP, GR, SH, LLD, LLS, AC, CNL, and DEN.

Fig. 12 presents the prediction outcomes of the five models for the JPH381-DY well. The initial five tracks in the figure exhibit conventional well logs, whereas the sixth track represents the permeability predictions of the five models. Among the five models, the TDCNNs-GRUs model displays the highest degree of overlap with the core measurement results, indicating the most reliable permeability prediction. Table 3 lists the prediction errors of the five models at the core sample location. The TDCNNs-GRUs model reveals the most exceptional predictive performance among the five models, with a correlation coefficient of 0.9262, and an MAE, MSE, and RMSE of 0.0851mD, 0.0108mD, and 0.1040mD, respectively.

The accurate determination of permeability in tight sandstone reservoirs remains a formidable challenge within the industry. In this study, we have addressed this challenge by introducing a novel deep learning model that integrates 2DCNN and GRU architectures. Our findings demonstrate a remarkable level of accuracy in predicting the permeability of tight sandstone reservoirs within the study area, thereby underscoring the efficacy of deep learning methodologies in forecasting parameters for unconventional reservoirs. Furthermore, the versatility of deep learning extends to the prediction of carbonate reservoir

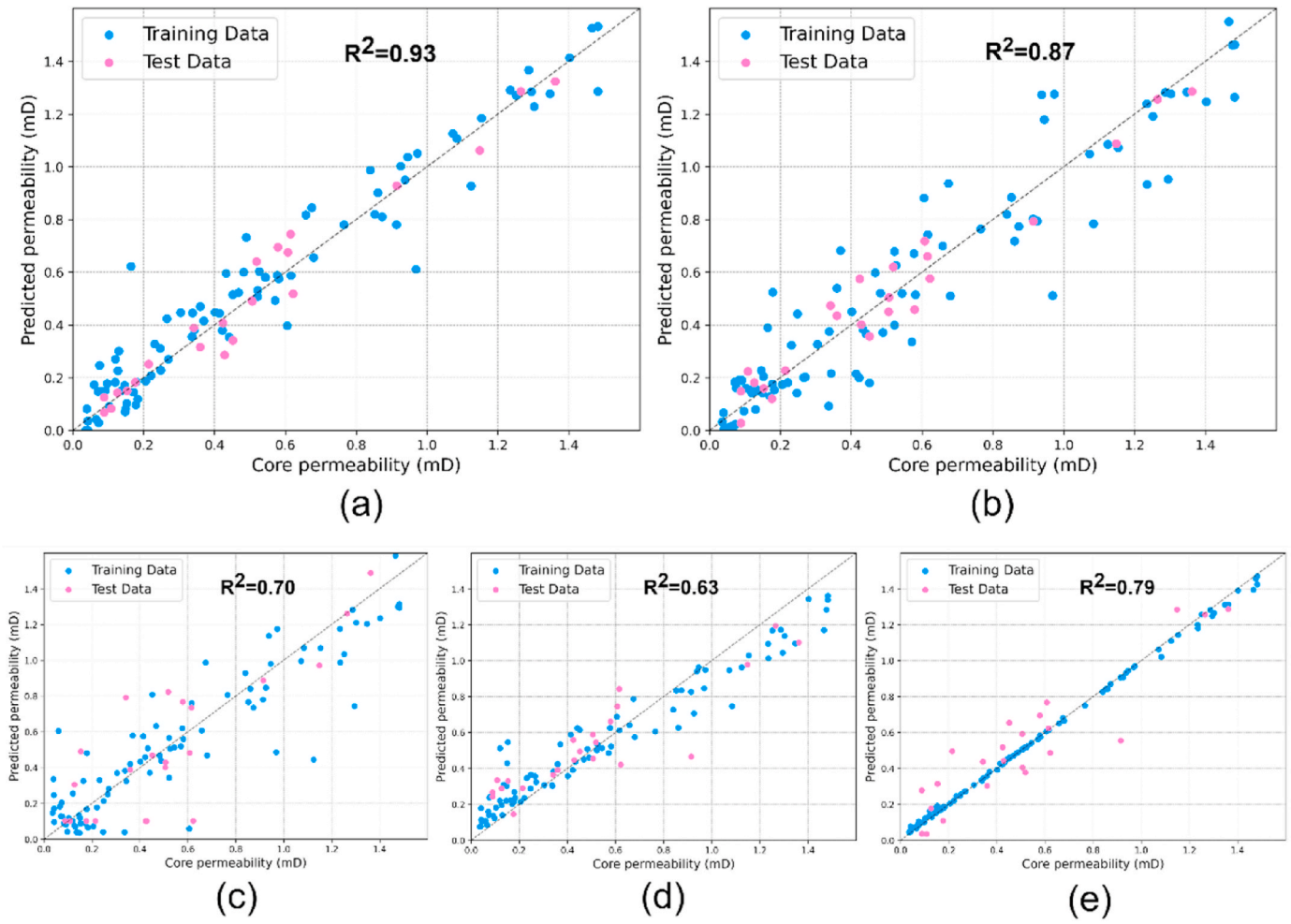

Fig. 11. Cross-plots displaying the predicted permeability of five different methods compared to true values and the R^2 for test data, with blue indicating training data and pink indicating test data. (a) Results of cross-plotting for the TDCNNs-GRUs model. (b) Results of cross-plotting for the 2-D CNNs model. (c) Results of cross-plotting for the GRUs model. (d) Results of cross-plotting for the SVM model. (e) Results of cross-plotting for the XGBoost model.

parameters, as evidenced by numerous studies (Tran et al., 2020; Sen et al., 2021b; Zhang et al., 2021b; Mohammadian et al., 2022; Zanganeh Kamali et al., 2022). We assert that the proposed methodology is equally adept at accurately predicting permeability in carbonate reservoirs. However, it is essential to acknowledge the inherent complexities associated with carbonate reservoirs (Wang et al., 2020c; Zhou et al., 2020b). These reservoirs exhibit diverse and intricate spatial characteristics, often characterized by heterogenous and the presence of multiple reservoir space types, such as pore types, fracture types, vug types and cave types, either individually or in combination (Farooq et al., 2019; Zhou et al., 2020b; Li et al., 2023a). Moreover, the permeability values within carbonate reservoirs can span several orders of magnitude. Consequently, when applying our method to carbonate reservoirs, careful attention must be paid to feature engineering and data modeling. In particular, differentiating between various reservoir space types is paramount. For instance, pore types, fracture types, vug types and cave types carbonate reservoirs typically manifest distinct well logs characteristics. Therefore, modeling these reservoir types separately, perhaps by training distinct sets of hyperparameters, often yields superior prediction outcomes. This approach ensures that the unique attributes of each reservoir space type are appropriately captured, leading to enhanced predictive accuracy. In summary, while our study showcases the effectiveness of our deep learning model in predicting permeability for tight sandstone reservoirs, its potential extends to the prediction of permeability in carbonate reservoirs.

5.3. *The significance of geological feature maps*

The fundamental principle of deep learning is that the quality of input data significantly impacts the accuracy of output data. However, in geoscience, the complexity and diversity of data coupled with the existence of multiple interpretation solutions can impede the utilization of deep learning algorithms in geological and geophysical data analysis. Thus, the importance of elaborate feature engineering preprocessing programs in fine-tuning input data cannot be overemphasized as this ensures accurate identification of crucial geological features and patterns relevant to the target geological application.

Geological feature maps, as seen in Figs. 6 and 7, lack physical meaning on the surface, and it is difficult to provide an intuitive explanation for geological feature images from a human perspective. Consequently, direct observation of such images does not provide any real physical scenarios relating to permeability. However, well logs offer valuable information regarding the physical properties of underground formation. For instance, the gamma ray logging measures the radioactive intensity in the formation and reflects the clay content. The clay composition, in turn, influences the permeability of the rock. Similarly, resistivity logging (LLD and LLS) provides information about fluid type and pore connectivity. The different logging curves have varying lateral detection depths. Integrating and transforming different logging data at the same depth point into a geological feature map can be considered a spatial representation of the comprehensive physical characteristics of the reservoir at that depth point. Prior studies and the current research

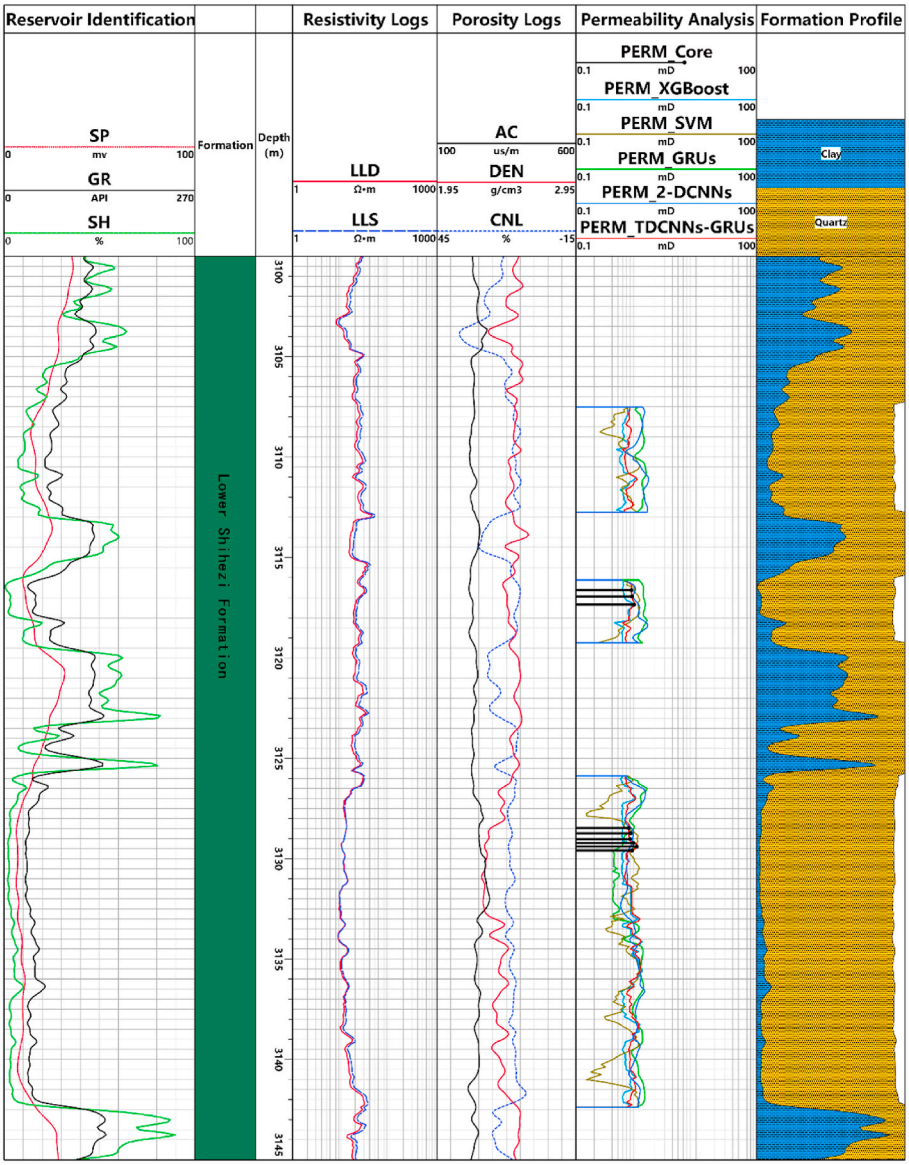

Fig. 12. Predicted permeability results using TDCNNs-GRUs model in JPH381-DY well of Lower Shihezi Formation in Hangjinqi area of Ordos Basin. The predicted permeability values exhibit strong agreement with the core measurements. The comparison of the permeability prediction results of track 6 reveals the superiority of the TDCNNs-GRUs method over the other four models.

Table 3
Permeability prediction errors for various methods in the JPH381-DY well.

Models	MAE (mD)	MSE (mD)	RMSE (mD)	R^2 (−)
Our proposed	0.0851	0.0108	0.1040	0.9262
2-D CNNs (Without GRUs)	0.0948	0.0211	0.1453	0.8575
GRUs (Without 2-D CNNs)	0.1644	0.0673	0.2594	0.3632
SVM	0.1393	0.0517	0.2274	0.4786
XGBoost	0.1156	0.0335	0.1829	0.5163

demonstrate that these images denote a specific category of geological patterns from the perspective of computers and deep learning algorithms (Zhong et al., 2019; Masroor et al., 2022). Furthermore, these geological patterns can reflect the intricate geological conditions beneath the surface and provide insights into the petrophysical characteristics of reservoirs.

Convolutional neural networks (CNNs) possess the ability to effectively extract multidimensional geological feature information of varying scales without losing vital data and superior capabilities in pattern recognition and image processing. The examination of the deep learning algorithm utilized in this paper reveals that the 2D-CNN can effectively extract multidimensional geological feature information of multiple scales contained in geological feature images. Following real and reasonable label data calibration, a deep nonlinear mapping relationship between high-dimensional features and target outputs can be established, thereby achieving precise predictions of various formation parameters such as permeability, porosity, and total organic carbon content.

5.4. Enhancing predictive performance through the integration of 2-D CNN and GRU architectures

In the pursuit of achieving optimal results, feature engineering is a critical aspect. However, it is also essential to consider the adaptability of data types to the characteristics of the model. Therefore, the interplay between data and the model is crucial to resolving the problem. To leverage the strengths of the two-dimensional convolutional neural network's (2-DCNN) feature extraction capabilities on geological

feature maps while retaining temporal feature information contained in logging data, we generate continuous geological feature images at specified time intervals and introduce the gated recurrent neural network. By using TimeDistributed layer wrapping technology, a functional coupling between 2-DCNNs and GRUs was achieved. Fig. 13 displays the residual plot between predicted permeability and prediction error in test well by our proposed TDCNNs-GRUs, 2-D CNN (without GRUs), and GRUs (without 2-D CNNs). The results show that our proposed method has the most uniform prediction error distribution, and the average error value is near zero, implying that TDCNNs-GRUs can learn the feature information effectively. In contrast, the input of the 2-DCNNs model only contains a single geological feature map, disregarding the temporal features of the logging curve, resulting in poor formation permeability prediction results. Although the input of the GRUs model is logging curve data with the same time step, it lacks potent feature extraction capabilities and struggles to establish a direct depth nonlinear mapping relationship between the original conventional logging curve and the formation permeability, resulting in unsurprisingly poor prediction results. Continuous geological feature maps capture the geological sedimentation process experienced by the formation in a specific time period and reflect the sedimentary evolution of the formation indirectly. Therefore, by combining the constructed geological feature map with the coupling of 2-DCNN and GRU, comprehensive data mining of logging data can be carried out in both the spatial and time dimensions, leading to accurate predictions of reservoir permeability.

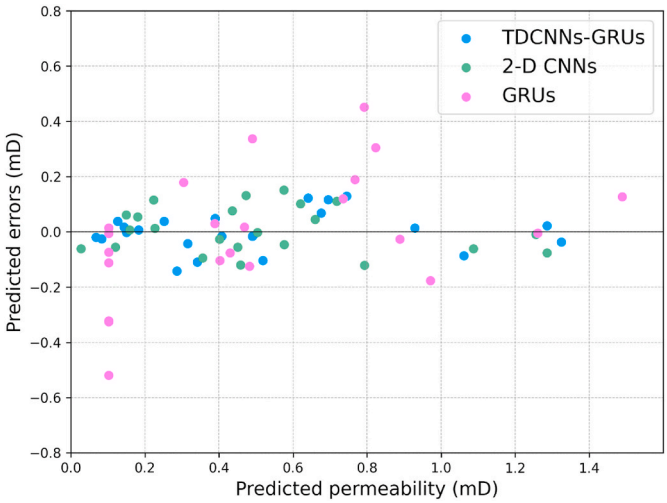

Fig. 13. Residual plots of prediction errors and predicted values of the three methods in permeability prediction.

6. Conclusions

Permeability is a crucial reservoir parameter in oil and gas exploration and development, and the development of accurate and cost-effective methods for permeability prediction has been a focus of research. In this paper, we propose a novel regression model, TDCNNs-GRUs, that integrates 2-D CNNs and GRUs to predict permeability in tight sandstone reservoirs. To preprocess input data, a method is introduced that converts conventional well logs into geological feature maps, which are then transformed into continuous feature maps with a specific time step as a sample. By incorporating TimeDistributed layer encapsulation technology, the model can efficiently extract spatial and temporal features from input data. The TDCNNs-GRUs benefits from the 2-D convolutional layers to capture spatial and robust features of the geological feature maps and utilized GRU units to implement holistic temporal features modeling. To validate the predictive performance of the proposed method, we divided TDCNNs-GRUs into two subnetwork models for comparative analysis, and two traditional machine learning models are also included for comparison. The results of the blind well test show that the proposed method has the lowest prediction error. Moreover, the permeability prediction results of core well reservoir segments also confirm the strong generalization and broad applicability of the proposed model. In conclusion, the proposed TDCNNs-GRUs model establishes a more complex nonlinear relationship between logging data and permeability, resulting in outstanding predictive performance and offering a valuable solution for permeability prediction in tight sandstone reservoirs.

CRediT authorship contribution statement

Yinhong Tian: Conceptualization, Data curation, Formal analysis, Investigation, Methodology, Software, Supervision, Validation, Visualization, Writing – original draft, Writing – review & editing, Project administration, Resources. **Guiwen Wang:** Conceptualization, Data curation, Formal analysis, Funding acquisition, Project administration, Resources, Supervision. **Hongbin Li:** Conceptualization, Formal analysis, Investigation, Validation, Visualization. **Yuyue Huang:** Project administration, Supervision. **Fei Zhao:** Project administration, Supervision. **Yunlong Guo:** Conceptualization, Data curation, Formal analysis, Methodology, Supervision. **Jie Gao:** Conceptualization, Data curation, Formal analysis, Funding acquisition, Project administration, Resources, Software, Supervision. **Jin Lai:** Conceptualization, Formal analysis, Project administration, Supervision, Writing – review & editing.

Declaration of competing interest

The authors declare that they have no known competing financial interests or personal relationships that could have appeared to influence the work reported in this paper.

Data availability

The data that has been used is confidential.

Acknowledgments

This work was supported by the National Natural Science Foundation of China (Grant No. 42002133, 42072150) for the financial support and permission to publish this paper. We appreciate the editorial staff and all four reviewers for their diligent work with enthusiasm and patience.

References

Afrasiabi, S., et al., 2021. Wide-area composite load parameter identification based on multi-residual deep neural network. IEEE Trans. Neural. Netw. Learn. Syst 34 (9), 6121–6131.
Ahmadi, M.A., 2015. Connectionist approach estimates gas–oil relative permeability in petroleum reservoirs: application to reservoir simulation. Fuel 140, 429–439.
Aïfa, T., 2014. Neural network applications to reservoirs: physics-based models and data models. J. Petrol. Sci. Eng. 123, 1–6.
Aïfa, T., Baouche, R., Baddari, K., 2014a. Neuro-fuzzy system to predict permeability and porosity from well log data: a case study of Hassi R′ Mel gas field. Algeria. J. Petrol. Sci. Eng. 123, 217–229.
Aïfa, T., Zerrouki, A.A., Baddari, K., Géraud, Y., 2014b. Magnetic susceptibility and its relation with fractures and petrophysical parameters in the tight sand oil reservoir of Hamra quartzites, southwest of the Hassi Messaoud oil field, Algeria. J. Petrol. Sci. Eng. 123, 120–137.
Al Khalifah, H., Glover, P., Lorinczi, P., 2020. Permeability prediction and diagenesis in tight carbonates using machine learning techniques. Mar. Petrol. Geol. 112, 104096.
Ali Ahmadi, M., Zendehboudi, S., Lohi, A., Elkamel, A., Chatzis, I., 2013. Reservoir permeability prediction by neural networks combined with hybrid genetic algorithm and particle swarm optimization. Geophys. Prospect. 61 (3), 582–598.
Ameur-Zaimeche, O., Kechiched, R., Heddam, S., Wood, D.A., 2022. Real-time porosity prediction using gas-while-drilling data and machine learning with reservoir associated gas: case study for Hassi Messaoud field, Algeria. Mar. Petrol. Geol. 140, 105631.

Anifowose, F., Abdulraheem, A., Al-Shuhail, A., 2019. A parametric study of machine learning techniques in petroleum reservoir permeability prediction by integrating seismic attributes and wireline data. J. Petrol. Sci. Eng. 176, 762–774.
Arif, S., Wang, J., Ul Hassan, T., Fei, Z., 2019. 3D-CNN-based fused feature maps with LSTM applied to action recognition. Future Internet 11 (2), 42.
Ba, J.L., Kiros, J.R., Hinton, G.E., 2016. Layer normalization. arXiv preprint arXiv: 1607.06450.
Babak, O., Resnick, J., 2016. On the use of particle-size-distribution data for permeability prediction. SPE. Reserv. Eval. Eng. 19 (1), 163–180.
Bai, Y., Tan, M., Shi, Y., Zhang, H., Li, G., 2022. Regression committee machine and petrophysical model jointly driven parameters prediction from wireline logs in tight sandstone reservoirs. IEEE Trans. Geosci. Remote. Sens. 60, 1–9.
Baouche, R., Aïfa, T., Baddari, K., 2017. Intelligent methods for predicting nuclear magnetic resonance of porosity and permeability by conventional well-logs: a case study of Saharan field. Arabian J. Geosci. 10, 1–21.
Bergen, K.J., Johnson, P.A., de Hoop, M.V., Beroza, G.C., 2019. Machine learning for data-driven discovery in solid Earth geoscience. Science 363 (6433), eaau0323.
Carman, P.C., 1997. Fluid flow through granular beds. Chem. Eng. Res. Des. 75, S32–S48.
Chen, J., et al., 2022. Full-stack machine learning development framework for energy industry applications, ADIPEC. OnePetro. SPE, D031S084R004.
Chen, X., et al., 2018. A new model of pore structure typing based on fractal geometry. Mar. Petrol. Geol. 98, 291–305.
Chen, Y., Zhang, D., 2020. Physics-constrained deep learning of geomechanical logs. IEEE Trans. Geosci. Remote. Sens. 58 (8), 5932–5943.
Cho, K., et al., 2014. Learning phrase representations using RNN encoder-decoder for statistical machine translation. arXiv preprint arXiv:1406.1078.
Chung, J., Gulcehre, C., Cho, K., Bengio, Y., 2014. Empirical evaluation of gated recurrent neural networks on sequence modeling. arXiv preprint arXiv:1412.3555.
Deighan, D.S., Field, S.E., Capano, C.D., Khanna, G., 2021. Genetic-algorithm-optimized neural networks for gravitational wave classification. Neural Comput. Appl. 33 (20), 13859–13883.
Dong, H., Wang, W., Huang, K., Coenen, F., 2021. Automated social text annotation with joint multilabel attention networks. IEEE Trans. Neural. Netw. Learn. Syst. 32 (5), 2224–2238.
Dong, S., et al., 2023. Fracture identification in reservoirs using well log data by window sliding recurrent neural network. Geoenergy Science and Engineering 230, 212165.
Dong, Y., et al., 2022. Cross orogenic belts in Central China: implications for the tectonic and paleogeographic evolution of the east asian continental collage. Gondwana Res. 109, 18–88.
El-Gendy, N.H., Radwan, A.E., Waziry, M.A., Dodd, T.J., Barakat, M.K., 2022. An integrated sedimentological, rock typing, image logs, and artificial neural networks analysis for reservoir quality assessment of the heterogeneous fluvial-deltaic Messinian Abu Madi reservoirs, Salma field, onshore East Nile Delta, Egypt. Mar. Petrol. Geol. 145, 105910.
Ercolano, G., Rossi, S., 2021. Combining CNN and LSTM for activity of daily living recognition with a 3D matrix skeleton representation. Intel. Serv. Robot. 14 (2), 175–185.
Farooq, U., et al., 2019. Heterogeneity in the petrophysical properties of carbonate reservoirs in Tal block. In: SPWLA 60th Annual Logging Symposium. OnePetro.
Fu, J., et al., 2023. Field application of a novel multi-resolution multi-well unconventional reservoir simulation: history matching and parameter identification. In: SPE/AAPG/SEG Unconventional Resources Technology Conference. URTEC, D021S049R001.
Gao, Q., et al., 2022. Flow-coupled-geomechanical modelling of CO2 transport in depleted shale from a microscopic perspective. Energy 257, 124727.
Ghazi, M.M., Sørensen, L., Ourselin, S., Nielsen, M., 2022. CARRNN: a continuous autoregressive recurrent neural network for deep representation learning from sporadic temporal data. IEEE Trans. Neural. Netw. Learn. Syst.
Girshick, R., Donahue, J., Darrell, T., Malik, J., 2014. Rich feature hierarchies for accurate object detection and semantic segmentation. In: Proceedings of the IEEE Conference on Computer Vision and Pattern Recognition, pp. 580–587.
Gu, Y., Bao, Z., Cui, G., 2018. Permeability prediction using hybrid techniques of continuous restricted Boltzmann machine, particle swarm optimization and support vector regression. J. Nat. Gas Sci. Eng. 59, 97–115.
Handhal, A.M., Al-Abadi, A.M., Chafeet, H.E., Ismail, M.J., 2020. Prediction of total organic carbon at Rumaila oil field, Southern Iraq using conventional well logs and machine learning algorithms. Mar. Petrol. Geol. 116, 104347.
Hassan, E., Shams, M.Y., Hikal, N.A., Elmougy, S., 2023. The effect of choosing optimizer algorithms to improve computer vision tasks: a comparative study. Multimed Tools Appl 82 (11), 16591–16633.
He, K., Zhang, X., Ren, S., Sun, J., 2016. Deep residual learning for image recognition. Proceedings of the IEEE Conference on Computer Vision and Pattern Recognition, pp. 770–778.
Hochreiter, S., Schmidhuber, J., 1997. Long short-term memory. Neural Comput. 9 (8), 1735–1780.
Huo, F., et al., 2022. Prediction of reservoir key parameters in 'sweet spot'on the basis of particle swarm optimization to TCN-LSTM network. J. Petrol. Sci. Eng. 214, 110544.
Iiduka, H., 2022. Appropriate learning rates of adaptive learning rate optimization algorithms for training deep neural networks. IEEE Trans. Cybern. 52 (12), 13250–13261.
Ikuta, M., Zhang, J., 2022. A deep convolutional gated recurrent unit for CT image reconstruction. IEEE Trans. Neural. Netw. Learn. Syst.
Kamali, M.Z., et al., 2022. Permeability prediction of heterogeneous carbonate gas condensate reservoirs applying group method of data handling. Mar. Petrol. Geol. 139, 105597.
Kardani, N., et al., 2021. Predicting permeability of tight carbonates using a hybrid machine learning approach of modified equilibrium optimizer and extreme learning machine. Acta. Geotech. 17 (4), 1239–1255.
Krizhevsky, A., Sutskever, I., Hinton, G.E., 2017. Imagenet classification with deep convolutional neural networks. Commun. ACM 60 (6), 84–90.
Li, H., et al., 2023a. Fault-Karst systems in the deep ordovician carbonate reservoirs in the yingshan Formation of tahe Oilfield tarim basin, China. Geoenergy Science and Engineering 231, 212338.
Li, W.-l., Wen-ming, J., Zhen, L., Ting, L., Jing-yu, Z., 2015. Control of boerjianghaizi fault on gas accumulation of upper paleozoic in northern Ordos Basin. Geoscience 29 (3), 584.
Li, X., Li, B., Liu, F., Li, T., Nie, X., 2023b. Advances in the application of deep learning methods to digital rock technology. Advances in Geo-Energy Research 8 (1).
Li, Z., Liu, F., Yang, W., Peng, S., Zhou, J., 2022. A survey of convolutional neural networks: analysis, applications, and prospects. IEEE Trans. Neural. Netw. Learn. Syst. 33 (12), 6999–7019.
Liu, J.-J., Liu, J.-C., Song, H., 2022. Permeability predictions for tight sandstone reservoir using explainable machine learning and particle swarm optimization. Geofluids 2022, 1–15.
Liu, K., et al., 2020. Tectonic controls on Permian tight gas accumulation: constrains from fluid inclusion and paleo-structure reconstruction in the Hangjinqi area, northern Ordos Basin, China. J. Nat. Gas Sci. Eng. 83, 103616.
Masroor, M., Emami Niri, M., Rajabi-Ghozloo, A.H., Sharifinasab, M.H., Sajjadi, M., 2022. Application of machine and deep learning techniques to estimate NMR-derived permeability from conventional well logs and artificial 2D feature maps. J. Pet. Explor. Prod. Te. 12 (11), 2937–2953.
Mohammadian, E., Kheirollahi, M., Liu, B., Ostadhassan, M., Sabet, M., 2022. A case study of petrophysical rock typing and permeability prediction using machine learning in a heterogenous carbonate reservoir in Iran. Sci. Rep-UK 12 (1), 4505.
Montaha, S., et al., 2022. TimeDistributed-CNN-LSTM: a hybrid approach combining CNN and LSTM to classify brain tumor on 3D MRI scans performing ablation study. IEEE Access 10, 60039–60059.
Mustafa, A., et al., 2022. Data-driven machine learning approach to predict mineralogy of organic-rich shales: an example from Qusaiba Shale, Rub'al Khali Basin, Saudi Arabia. Mar. Petrol. Geol. 137, 105495.
Nagao, M., Yao, C., Onishi, T., Chen, H., Datta-Gupta, A., 2023. An efficient deep learning-based workflow for CO2 plume imaging with distributed pressure and temperature measurements. SPE J. 1–15.
Niu, D.-M., et al., 2022. Multi-scale classification and evaluation of shale reservoirs and 'sweet spot'prediction of the second and third members of the Qingshankou Formation in the Songliao Basin based on machine learning. J. Petrol. Sci. Eng. 216, 110678.
Osogba, O., Misra, S., Xu, C., 2020. Machine learning workflow to predict multi-target subsurface signals for the exploration of hydrocarbon and water. Fuel 278, 118357.
Otchere, D.A., Ganat, T.O.A., Gholami, R., Lawal, M., 2021. A novel custom ensemble learning model for an improved reservoir permeability and water saturation prediction. J. Nat. Gas Sci. Eng. 91, 103962.
Ou, Y., Li, L., Li, D., Zhang, J., 2022. ESRM: an efficient regression model based on random kernels for side channel analysis. Int. J. Mach. Learn. Cyb. 13 (10), 3199–3209.
Puentes G, D.E., Barrios H, C.J., Navaux, P.O.A., 2022. Hyperparameter optimization for convolutional neural networks with genetic algorithms and bayesian optimization. In: 2022 IEEE Latin American Conference on Computational Intelligence (LA-CCI), pp. 1–5.
Qiao, H., Wang, T., Wang, P., Qiao, S., Zhang, L., 2018. A time-distributed spatiotemporal feature learning method for machine health monitoring with multi-sensor time series. Sensors-Basel 18 (9), 2932.
Qin, Z., et al., 2020. A novel method to obtain permeability in a dual-pore system using geophysical logs: a case study of an upper triassic formation, southwest Ordos Basin, China. Nat. Resour. Res. 29 (4), 2619–2634.
Qiu, L., Xiangji, M., Hao, L., 2019. Characteristics of detritus development in the Permian lower Shihezi Formation in Hangjinqi area and its influence on reservoir physical properties. Oil Gas Geol. 40 (1), 24–33.
Rafik, B., Kamel, B., 2017. Prediction of permeability and porosity from well log data using the nonparametric regression with multivariate analysis and neural network, Hassi R'Mel Field, Algeria. Egyptian Journal of Petroleum 26 (3), 763–778.
Raji, I.D., et al., 2022. Simple deterministic selection-based genetic algorithm for hyperparameter tuning of machine learning models. Appl. Sci. 12 (3), 1186.
Ravandi, E.G., Nezamabadi-Pour, H., Monfared, A.E.F., Jaafarpour, A.M., 2014. Reservoir characterization by a combination of fuzzy logic and genetic algorithm. Petrol. Sci. Technol. 32 (7), 840–847.
Ronneberger, O., Fischer, P., Brox, T., 2015. U-net: convolutional networks for biomedical image segmentation. In: Medical Image Computing and Computer-Assisted Intervention–MICCAI 2015: 18th International Conference, Munich, Germany, October 5-9, 2015, Proceedings, Part III 18. Springer, pp. 234–241.
Sakhavi, S., Guan, C., Yan, S., 2018. Learning temporal information for brain-computer interface using convolutional neural networks. IEEE Trans. Neural. Netw. Learn. Syst. 29 (11), 5619–5629.
Saporetti, C., Fonseca, D., Oliveira, L., Pereira, E., Goliatt, L., 2022. Hybrid machine learning models for estimating total organic carbon from mineral constituents in core samples of shale gas fields. Mar. Petrol. Geol. 143, 105783.
Sen, S., et al., 2021a. Petrophysical heterogeneity of the early Cretaceous Alamein dolomite reservoir from North Razzak oil field, Egypt integrating well logs, core measurements, and machine learning approach. Fuel 306, 121698.

Sen, S., et al., 2021b. Petrophysical heterogeneity of the early Cretaceous Alamein dolomite reservoir from North Razzak oil field, Egypt integrating well logs, core measurements, and machine learning approach. Fuel 306.
Seyyedattar, M., Zendehboudi, S., Butt, S., 2021. Relative permeability modeling using extra trees, ANFIS, and hybrid LSSVM–CSA methods. Nat. Resour. Res. 31 (1), 571–600.
Shi, S., et al., 2023. Acoustic impedance inversion in coal strata using the priori constraint-based TCN-BiGRU method. Advances in Geo-Energy Research 9 (1).
Srivastava, N., Hinton, G., Krizhevsky, A., Sutskever, I., Salakhutdinov, R., 2014. Dropout: a simple way to prevent neural networks from overfitting. The journal of machine learning research 15 (1), 1929–1958.
Sudakov, O., Burnaev, E., Koroteev, D., 2019. Driving digital rock towards machine learning: predicting permeability with gradient boosting and deep neural networks. Comput. Geosci-Uk. 127, 91–98.
Sun, J., et al., 2023. Ordovician tectonic transition from passive margin into peripheral foreland in the southern Ordos: a diagnostic insight into the closure of Erlangping Ocean between the North Qinling Arc and North China Block. Basin Res. 35 (1), 336–362.
Tan, X., et al., 2023. Sedimentary characteristics of sandy braided river deposits and factors controlling their deposition: a case study of the lower Shihezi Formation in the northern ordos basin, China. Geoenergy Science and Engineering, 211932.
Tran, H., Kasha, A., Sakhaee-Pour, A., Hussein, I., 2020. Predicting carbonate formation permeability using machine learning. J. Petrol. Sci. Eng. 195, 107581.
Wang, J., Cao, J., 2021. Deep learning reservoir porosity prediction using integrated neural network. Arab. J. Sci. Eng. 47 (9), 11313–11327.
Wang, J., Cao, J., You, J., Cheng, M., Zhou, P., 2021. A method for well log data generation based on a spatio-temporal neural network. J. Geophys. Eng. 18 (5), 700–711.
Wang, J., Cao, J., Yuan, S., 2022. Deep learning reservoir porosity prediction method based on a spatiotemporal convolution bi-directional long short-term memory neural network model. Geomech. Energy. Envir. 32, 100282.
Wang, R., Li, C., Fu, W., Tang, G., 2020a. Deep learning method based on gated recurrent unit and variational mode decomposition for short-term wind power interval prediction. IEEE Trans. Neural. Netw. Learn. Syst. 31 (10), 3814–3827.
Wang, R., et al., 2020b. Clay mineral content, type, and their effects on pore throat structure and reservoir properties: insight from the Permian tight sandstones in the Hangjinqi area, north Ordos Basin, China. Mar. Petrol. Geol. 115, 104281.
Wang, S., et al., 2020c. Logging identification and evaluation of vertical zonation of buried hill in Cambrian dolomite reservoir: a study of Yingmai-Yaha buried hill structural belt, northern Tarim basin. J. Petrol. Sci. Eng. 195, 107758.
Wu, J., Yin, X., Xiao, H., 2018. Seeing permeability from images: fast prediction with convolutional neural networks. Sci. Bull. 63 (18), 1215–1222.
Wu, L., Dong, Z., Li, W., Jing, C., Qu, B., 2021. Well-logging prediction based on hybrid neural network model. Energies 14 (24), 8583.
Xiao, X., Zhao, B., Thu, Z., Song, Z., Wilkins, R., 2005. Upper paleozoic petroleum system, Ordos basin. China. Mar. Petrol. Geol. 22 (8), 945–963.
Xu, Q., et al., 2018. Inversion and propagation of the late paleozoic porjianghaizi fault (north Ordos Basin, China): controls on sedimentation and gas accumulations. Mar. Petrol. Geol. 91, 706–722.
Yang, L., et al., 2022. High-fidelity permeability and porosity prediction using deep learning with the self-attention mechanism. IEEE Trans. Neural. Netw. Learn. Syst.
Yang, P., et al., 2021. Diagenetic history and reservoir evolution of tight sandstones in the second member of the Upper Triassic Xujiahe Formation, western Sichuan Basin, China. J. Petrol. Sci. Eng. 201, 108451.
Yang, W., Xia, K., Fan, S., 2023. Oil logging reservoir recognition based on TCN and SA-BiLSTM deep learning method. Eng. Appl. Artif. Intell. 121, 105950.
Yang, Y., Li, W., Ma, L., 2005. Tectonic and stratigraphic controls of hydrocarbon systems in the Ordos basin: a multicycle cratonic basin in central China. AAPG Bull. 89 (2), 255–269.
Yao, C., et al., 2021. Robust CO2 plume imaging using joint tomographic inversion of distributed pressure and temperature measurements. In: SPE Annual Technical Conference and Exhibition? SPE, D021S023R006.
Yao, C., et al., 2023. Machine learning based FPSO topsides weight estimation for a Project on an early stage. In: Offshore Technology Conference. OTC, D011S004R001.
Yu, Q., et al., 2020. Identification of rock pore structures and permeabilities using electron microscopy experiments and deep learning interpretations. Fuel 268, 117416.
Zanganeh Kamali, M., et al., 2022. Permeability prediction of heterogeneous carbonate gas condensate reservoirs applying group method of data handling. Mar. Petrol. Geol. 139.
Zhang, G., et al., 2018. Permeability prediction of isolated channel sands using machine learning. J. Appl. Geophy. 159, 605–615.
Zhang, H., et al., 2022. Permeability prediction of low-resolution porous media images using autoencoder-based convolutional neural network. J. Petrol. Sci. Eng. 208, 109589.
Zhang, L., et al., 2017. Hydrothermal mineralization in the sandstone–hosted Hangjinqi uranium deposit, North Ordos Basin, China. Ore Geol. Rev. 80, 103–115.
Zhang, Z., Zhang, H., Li, J., Cai, Z., 2021a. Permeability and porosity prediction using logging data in a heterogeneous dolomite reservoir: an integrated approach. J. Nat. Gas Sci. Eng. 86, 103743.
Zhang, Z., Zhang, H., Li, J., Cai, Z., 2021b. Permeability and porosity prediction using logging data in a heterogeneous dolomite reservoir: an integrated approach. J. Nat. Gas Sci. Eng. 86.
Zhao, X., et al., 2022. Logging-data-driven permeability prediction in low-permeable sandstones based on machine learning with pattern visualization: a case study in Wenchang A Sag, Pearl River Mouth Basin. J. Petrol. Sci. Eng. 214, 110517.
Zheng, W., et al., 2021. Electrofacies classification of deeply buried carbonate strata using machine learning methods: a case study on ordovician paleokarst reservoirs in Tarim Basin. Mar. Petrol. Geol. 123, 104720.
Zhong, Z., Carr, T.R., Wu, X., Wang, G., 2019. Application of a convolutional neural network in permeability prediction: a case study in the Jacksonburg-Stringtown oil field, West Virginia, USAPermeability prediction via a CNN. Geophysics 84 (6), B363–B373.
Zhou, K., et al., 2020a. Fast prediction of reservoir permeability based on embedded feature selection and LightGBM using direct logging data. Meas. Sci. Technol. 31 (4).
Zhou, Y., Yang, F., Ji, Y., Zhou, X., Zhang, C., 2020b. Characteristics and controlling factors of dolomite karst reservoirs of the Sinian Dengying Formation, central Sichuan Basin, southwestern China. Precambrian Res. 343, 105708.
Zhu, Y., Iiduka, H., 2021. Unified algorithm framework for nonconvex stochastic optimization in deep neural networks. IEEE Access 9, 143807–143823.
Zou, C., et al., 2013. Continuous hydrocarbon accumulation over a large area as a distinguishing characteristic of unconventional petroleum: the Ordos Basin, North-Central China. Earth Sci. Rev. 126, 358–369.